MODELING AND CONTROL OF A BIOCHEMICAL LOOP REACTOR WITH CELL MASS RECYCLE

Ying Zhao and Sigurd Skogestad*
Department of Chemical Engineering, University of Trondheim - NTH
N-7034 Trondheim, Norway

Presented at AIChE Annual Meeting, San Francisco, Nov. 13-18, 1994.

Paper 39d

Abstract

This work is based on an industrial application of a biochemical loop reactor with cell mass recycle. In this paper the general features of this application are studied. The control objective for this biochemical process is to maintain cell concentration at the desired high concentration in order to maximize the production of cell mass.

In this work simple frequency-dependent tools such as the relative gain array (RGA) and the closed loop disturbance gain (CLDG) are used for control structure selection and controllability analysis with respect to disturbance rejection, and we study the effect of changes in the operating point on the choice of control structure as well as the possibility of partial control of this loop reactor. The optimization of cell productivity is also discussed.

In this biochemical process we have two available on-line measurements of secondary variables: CO_2 concentration and the base addition rate which are related to the cell growth rate. Based on the developed estimation model in this work that describes cell concentration as a function of the CO_2 concentration and the base addition rate, cell concentration can be on-line estimated from these two on-line measurements by applying the extended Kalman filter. From simulation results, a good agreement is observed between the true values and the estimated values.

*Author to whom correspondence should be addressed. Fax: 47-73-594080. E-mail: skoge@kjemi.unit.no

1 Introduction

The studied biochemical process is the propionic acid bacteria fermentation process. Propionic acid bacteria have long been used in the dairy industry. These bacteria play important roles in the development of the characteristic flavor and "eyes" production in Swiss-type cheeses as they ferment lactic acid with the production of propionic acid and carbon dioxide. Thus there is a strong interest in food industry to continuously obtain the propionic acid bacteria with high concentration at the maximum production rate. To attain this, the development of efficient on-line computer control system is essential.

A schematic overview of this continuous fermentation process is shown in Fig. 1. There are three streams into this loop reactor, that is, yeast extract (YE) acts as nitrogen source for incorporation into cell mass synthesis, lactic acid (LA) acts as both energy source for cell growth and carbon source for incorporation into cell mass synthesis (F_{in2}), the third inflow (F_{in3}) is base solution which is used for compensating pH change in the loop reactor. The reactor effluent is fed to a filter which is used for increasing the cell concentration by bleeding off a little used media at flow rate F_{filter}, and a part of the filter effluent including cell mass, organic acids and media is recycled to the bioreactor. F_{out} denotes the product stream flow rate. The operation objective of this process is to get high concentration cultivation of propionic acid bacteria in this loop reactor with cross-flow filtration.

In this work simple frequency-dependent tools such as the relative gain array (RGA) and the closed loop disturbance gain (CLDG) are used for control structure selection and controllability analysis with respect to disturbance rejection, and we study the effect of the parametric uncertainty in the model and changes in the operating point on the choice of control structure as well as the possibility of partial control of this loop reactor. The optimization of cell productivity is also discussed.

The knowledge of fermentation process state variables is crucial in any type of control scheme. Unfortunately, on-line measurement of the important state variables in fermentations, particularly cell concentration, remains a difficult problem. However a number of secondary or environmental variables can be on-line measured conventionally, such as pH, and CO_2 and O_2 in the exhaust gas. In propionic acid bacteria fermentation, CO_2 is the only gas produced. Further the CO_2 concentration is related to the cell growth rate. We have another available on-line measurement of secondary variable, that is base addition rate which is found to be possibly also related to the cell growth rate from experiment data analysis. Therefore based on the developed estimation model in this work that describes cell concentration as the function of the CO_2 concentration and base addition rate, cell concentration is on-line estimated from these two on-line measurements by applying the extended Kalman filter.

2 The dynamical model of process used in this work

The following assumptions are made during the further discussion:

1. The concentrations of cell mass, substrates, and dissolved carbon dioxide in the medium are uniform respectively in the whole loop (filter-fermenter) system.

2. The bioreactor volume is constant as it is well known that the cell growth kinetic effects in biological processes are far slower than the hydrodynamic effects.

Based on mass balances and the above assumptions, the dynamic model of process is derived as following:

$$\frac{dx}{dt} = \mu x - \frac{F_{out}}{V} x \tag{1}$$

$$\frac{dS_L}{dt} = -\frac{1}{Y_{x/L}} \mu x - \frac{F_{filter} + F_{out}}{V} S_L + \frac{F_{in2} S_{fL}}{V} \tag{2}$$

$$\frac{dS_Y}{dt} = -\frac{1}{Y_{x/Y}} \mu x - \frac{F_{filter} + F_{out}}{V} S_Y + \frac{F_{in1} S_{fY}}{V} \tag{3}$$

$$\frac{dc}{dt} = \frac{1}{Y_{x/co_2}} \mu x - \frac{F_{filter} + F_{out}}{V} c - \frac{F_7}{V} \rho_{CO_2} \tag{4}$$

where

x— Cell concentration

S_Y— Yeast Extract (YE) concentration, YE acts as growth-limiting substrate.

S_{fY}— the feed yeast extract concentration.

S_L— Lactic Acid (LA) concentration, LA is used as nonlimiting substrate.

S_{fL}— the feed lactic acid concentration.

V— Reactor volume.

c— dissolved carbon dioxide concentration in the medium.

F_7— carbon dioxide evolution rate in the exhaust gas.

ρ_{CO_2}— carbon dioxide gas density.

$Y_{x/L}$— the cell yield coefficient on the carbon energy source (LA).

$Y_{x/Y}$— the cell yield coefficient on the nitrogen source (YE).

Y_{x/co_2}— the cell yield coefficient on the carbon dioxide.

μ— the specific cell growth rate.

The specific cell growth rate is assumed to be expressed as the well-known Monod model such that

$$\mu = \mu_m \frac{s}{K_s + s}$$

where μ_m and K_s represent the maximum specific cell growth rate and the saturation constant respectively.

3 Measures for evaluating controllability

In the following we will use a plant description of the form

$$y(s) = G(s)u(s) + G_d(s)d(s) \tag{5}$$

where G and G_d denote the process and disturbance model and y, u and d are the outputs, manipulated inputs and disturbances, respectively.

In this paper we mainly use the relative gain array (RGA or Λ) as a measure of interaction and as a tool for control structure selection. The properties of the RGA are well known. The most

important for our purpose is that the RGA depends on the plant model only and is independent of scaling in inputs or outputs. For $n \times n$ plant $G(s)$ the RGA matrix can be computed using the formula

$$\Lambda(s) = G(s) \times [G^{-1}(s)]^T \tag{6}$$

where the $\times$ symbol denotes element by element multiplication (Hadamard product).

To evaluate the disturbance sensitivity, we consider the closed loop disturbance gain (CLDG) which is the appropriate measure when we use decentralized control (Hovd and Skogestad, 1992). For a disturbance d_k and an output y_i, the CLDG is defined by

$$\delta_{ik}(s) = g_{ii}(s)[G(s)^{-1}G_d(s)]_{ik} \tag{7}$$

A matrix of CLDG's may be computed from

$$\Delta(s) = \{\delta_{ik}\} = G_{diag}(s)G^{-1}(s)G_d(s) \tag{8}$$

where G_{diag} consists of the diagonal elements of G. The CLDG is scaling dependent, as it depends on the expected magnitude of disturbances and outputs. Actually, this is reasonable since the CLDG is a performance measure, which generally is scaling dependent.

3.1 Summary of controllability rules

We shall use the following rules for control structure selection and controllability analysis in this paper:

Rule 1. Avoid plants (designs) with large RGA-values (in particular at frequencies near cross-over). This rule applies for any controller, not only to decentralized control (Skogestad and Morari, 1987b).

Rule 2. Avoid *pairings ij* with negative values of the steady-state RGA, $\lambda_{ij}(0)$ (Grosdidier et al., 1985).

Rule 3. Prefer *pairings ij* where $g_{ij}(s)$ puts minimal restrictions on the achievable bandwidth for this loop, that is, avoid pairing with "significant" RHP-zeros (RHP-zeros close to the origin) in $g_{ij}(s)$ because otherwise this loop may go unstable if left by itself (with the other loops open) when decentralized controllers are used.

4 Case study

4.1 Steady state behavior

From eqs. (1-3), the steady state values of cell and substrate concentrations can be calculated:

$$\frac{dx}{dt} = 0 \Longrightarrow \mu = \frac{F_{out}}{V} \Longrightarrow S_Y = \frac{K_s F_{out}}{\mu_m V - F_{out}} \tag{9}$$

$$\frac{dS_L}{dt} = 0 \Longrightarrow S_L = \frac{F_{in2}S_{fL} - \frac{F_{out}x}{Y_{x/L}}}{F_{filter} + F_{out}} \tag{10}$$

$$\frac{dS_Y}{dt} = 0 \Longrightarrow x = \frac{F_{in1}S_{fY} - (F_{filter} + F_{out})S_Y}{F_{out}} Y_{x/Y} \tag{11}$$

The steady-state relationships are shown in Fig. (2-5).

As can be seen from eq. (9) and also Fig. (2-5), the steady-state growth-limiting substrate concentration (S_Y) is independent of its feed flow rate (F_{in1}). This unusual feature is due to the autocatalytic reaction. Thus S_Y depends only on the production rate (F_{out}). Another phenomena caused by the autocatalytic reaction is the possibility for washout. Physically, when F_{out} reaches to a critical value $F_{out_{max}}$ which can be calculated from eq. (11), the cell can not grow fast enough to keep up with its outflow, and the culture is washed out of the reactor.

1. The steady state relationship between the cell concentration (x) and the cell production rate (F_{out})

As shown in Fig. 2, when F_{out} increases the cell concentration (x) decreases and the limiting substrate concentration (S_Y) increases. Changes in F_{out} is balanced by adjusting F_{in2} in order to keep V constant. If F_{out} reaches to a critical value $F_{out_{max}}$, the culture is washed out of the reactor and substrate concentrations rises to their maximum ($S_Y = \frac{F_{in1}S_{fY}}{F_{filter}+F_{out_{max}}}$ and $S_L = \frac{F_{in2}S_{fL}}{F_{filter}+F_{out_{max}}}$). In this case, flow rates F_{in1}, F_{in3} and F_{filter} are constant.

2. The steady state relationship between the cell concentration (x) and the growth-limiting substrate feed flow rate (F_{in1})

When flow rates F_{in2}, F_{in3} and F_{out} are constant, x is proportional to F_{in1} as shown in Fig. 3. The changes in F_{in1} is compensated by adjusting F_{filter} to keep V constant. S_L decreases with increasing F_{in1} when F_{in2} is constant and then this gives a upper bound to F_{in1} so that S_L should not be decreased to its growth-limiting level. On the other hand, F_{in1} should be above a critical value $F_{in1_{min}}$. Otherwise at very low feed flow rates, a large fraction of cells may die from starvation, since the limiting substrate is not being added fast enough to permit maintenance of cell growth.

3. The steady state relationship between the cell concentration (x) and the non-limiting substrate feed flow rate (F_{in2})

In this case flow rates F_{in1}, F_{in3} and F_{out} are constant. x is insensitive to the changes in F_{in2} as shown in Fig. 4. Of course S_L increases with increasing F_{in2}. There also exists a lower bound to F_{in2}, i.e., F_{in2} should be above $F_{in2_{min}}$, otherwise $S_L = 0$. On the other hand, F_{in2} should be below F_{in2}, otherwise washout occurs.

4. The steady state relationship between the cell concentration (x) and the filtrate flow rate (F_{filter})

In this case flow rates F_{in1}, F_{in3} and F_6 are constant. The steady state behavior is very similar to case 3, x is insensitive to the changes in F_{filter} as shown in Fig. 5. S_L increases with increasing F_{filter} and this gives lower bound to F_{filter} so that S_L should be above its growth-limiting level. There also exists a upper bound to F_{filter}, i.e., F_{filter} should be below $F_{filter_{max}}$, otherwise washout occurs. $F_{filter_{max}}$ will decreases as K_s increases.

In total conclusion, in this biochemical loop reactor with multiple substrate streams the cell concentration is much more sensitive to changes in F_{out}, which is the main difference between this loop reactor with cell mass recycle and a general biochemical CSTR with single substrate stream where throughout most of the range of the dilution rates but not higher close to the critical value $D_{washout}$ the cell concentration almost remains constant. The steady state relationship between the cell concentration (x) and the nonlimiting substrate feed flow rate (F_{in2}) and the steady state relationship between the cell concentration (x) and the filtrate flow rate (F_{filter}) are very similar to each other, i.e., flow rates F_{in2} and F_{filter} have almost same effect on the state variables such as x, S_L and S_Y.

4.2 Maximization of cell productivity

As for many continuous bioreactors, the operation objective in this loop reactor is to maximize the cell productivity P. At steady state,

$$S_Y = \frac{K_s F_{out}}{\mu_m V - F_{out}}$$

As $S_Y > 0$, we should have $F_{out} < \mu_m V$.

$$x = \frac{F_{in1} S_{fY} - (F_{filter} + F_{out}) S_Y}{F_{out}} Y_{x/Y}$$

As $x > 0$, we should have $F_{out} < F_{out_{max}}$, otherwise washout occurs.

$$P = \frac{F_{out} x}{V} = \frac{Y_{x/Y}}{V} [F_{in1} S_{fY} - (F_{filter} + F_{out}) \frac{K_s F_{out}}{\mu_m V - F_{out}}] \tag{12}$$

Case 1. F_{out} increased and F_{in1} unchanged

In this case, other flow rates are unchanged except F_{in2} which is adjusted to balance changes in F_{out} in order to keep V constant. The cell concentration x will decrease with the increasing F_{out}. The total effect on P is

$$\frac{dP}{dF_{out}} = -\frac{Y_{x/Y}}{V} [\frac{K_s F_{out}}{\mu_m V - F_{out}} + (F_{filter} + F_{out}) \frac{K_s \mu_m V}{(\mu_m V - F_{out})^2}] < 0$$

Therefore increasing F_{out} will result in the decrease in P, no optimal value exists as shown in Fig. 6 (dashed curves).

Case 2. F_{out} increased and F_{in1} changed to keep x constant

If we use F_{in1} to control x at the desired higher concentration x_0, that is, increasing F_{in1} simultaneously with the increased F_{out},

$$F_{in1} = \frac{\frac{F_{out} x_0}{Y_{x/Y}} + (F_{in2} + F_{in3}) S_Y}{S_{fY} - S_Y}$$

Then in the case of x constant by increasing F_{in1}, to maximize the cell productivity ($P = \frac{F_{out} x_0}{V}$), we just increase F_{out} but below its critical value $F_{out_{max}}$. In this case, there is also no optimal value. The achievable high cell productivity is limited by the allowed maximum changes in flow rates F_{in1} and F_{out} as shown in Fig. 6 (solid curves).

Comparing these two cases, when F_{in1} varying with F_{out} such that x is kept constant at high concentration, higher cell productivity is obtained than in case 1. **We concluded** that in the loop reactor the better way to get as higher as possible cell productivity is to increase F_{out} together with adjusting F_{in1} to keep x at the desired high concentration.

4.3 Control structure selection and controllability analysis

In this biochemical loop reactor the main control objective is to control cell concentration x constant at high concentration. We have three output variables x, S_L and S_Y, the most important controlled output of them is x. In addition to possible disturbances in the manipulated inputs, we have included disturbances in the model parameters $Y_{x/Y}$, K_s and μ_m which may stem from variations in the environment conditions such as temperature, pH, aeration rate etc. Now we consider the operating variables in this biochemical loop reactor with cell mass recycle. In any scheme the number of controlled outputs must be less than or equal to the number of independent (manipulated) variables. In this loop reactor we have five manipulated inputs as shown in Fig. 1. Since the

pH is already controlled by the base addition rate F_{in3} and the reactor volume is assumed constant such that $F_{in1} + F_{in2} + F_{in3} = F_{filter} + F_{out}$, three independent manipulated variables (F_{in1}, F_{in2} and F_{out} or F_{in1}, F_{filter} and F_{out}) remain. Generally large flow rates are used to control reactor volume, then we have two alternative manipulated inputs F_{in2} and F_{filter} for volume control and therefore two alternative control strategies exist for controlling this loop reactor:

Alternative control strategy 1:

$$y = \begin{bmatrix} x \\ S_L \\ S_Y \end{bmatrix}; \quad u = \begin{bmatrix} F_{in1} \\ \mathbf{F_{in2}} \\ F_{out} \end{bmatrix}; \quad d = \begin{bmatrix} F_{in1_d} \\ F_{in2_d} \\ F_{out_d} \\ Y_{x/Y} \\ K_s \\ \mu_m \end{bmatrix}$$

Alternative control strategy 2:

$$y = \begin{bmatrix} x \\ S_L \\ S_Y \end{bmatrix}; \quad u = \begin{bmatrix} F_{in1} \\ \mathbf{F_{filter}} \\ F_{out} \end{bmatrix}; \quad d = \begin{bmatrix} F_{in1_d} \\ F_{filter_d} \\ F_{out_d} \\ Y_{x/Y} \\ K_s \\ \mu_m \end{bmatrix}$$

Scaling of variables

The allowed maximum output changes are

$$\bar{\Delta}x = 10\%\,\bar{x}; \quad \bar{\Delta}S_L = 30\%\,\bar{S}_L; \quad \bar{\Delta}S_Y = 20\%\,\bar{S}_Y$$

The allowed maximum input changes are

$$\bar{\Delta}F_{in1} = 30\%\,\bar{F}_{in1}; \quad \bar{\Delta}F_{in2} = 30\%\,\bar{F}_{in2}; \quad \bar{\Delta}F_{filter} = 30\%\,\bar{F}_{filter}; \quad \bar{\Delta}F_{out} = 30\%\,\bar{F}_{out}$$

The expected maximum disturbance changes are

$$\bar{\Delta}F_{in1_d} = 20\%\,\bar{\Delta}F_{in1}; \quad \bar{\Delta}F_{in2_d} = 20\%\,\bar{\Delta}F_{in2}; \quad \bar{\Delta}F_{filter_d} = 20\%\,\bar{\Delta}F_{filter}; \quad \bar{\Delta}F_{out_d} = 20\%\,\bar{\Delta}F_{out}$$

$$\bar{\Delta}Y_{x/Y} = 10\%\,\bar{Y}_{x/Y}; \quad \bar{\Delta}K_s = 10\%\,\bar{K}_s; \quad \bar{\Delta}\mu_m = 10\%\,\bar{\mu}_m$$

The scaled transfer matrices are derived by scaling all variables with respect to their maximum allowed changes.

In the following the overbar ($^-$) used to denote steady-state values will be deleted to simplify notation.

This loop reactor has no poles or transmission zeros in the right half plane (RHP). Therefore the loop reactor is stable at all nontrivial steady states. There are no fundamental problems related with instability, inverse responses or inherent bandwidth limitations.

Although a number of operating points ("case") have been studied, our findings can be illustrated by the two cases as given in Table 1.

Table 1: Steady State Data

Operating Point	F_{in1} (l/h)	F_{in2} (l/h)	F_{out} (l/h)	x (g/l)	S_L (g/l)	S_Y (g/l)	K_s (g/l)	$Y_{x/Y}$ (g/g)	$Y_{x/Y}$ (g/g)	μ_m (h^{-1})
No. I	0.684	18.229	0.365	29.429	0.2063	0.1333	0.0343	0.08	0.05	0.141
No. II	0.889	21.890	0.438	29.429	0.2063	0.7273	0.0343	0.08	0.05	0.141

4.3.1 Operating Point I

In this operating point the cell growth is substrate limited and the parameter K_s value is very low. At first comparing these two alternative control strategies, the steady-state gain matrices in terms of scaled variables are respectively:

$$G_1(0) = \begin{bmatrix} 3.06 & -0.05 & -3.28 \\ -55.89 & 55.89 & 5.05 \\ 0.00 & 0.00 & 7.33 \end{bmatrix}; \quad G_2(0) = \begin{bmatrix} 3.06 & -0.06 & -3.28 \\ -57.98 & 57.07 & 6.17 \\ 0.00 & 0.00 & 7.33 \end{bmatrix}$$

We first note that in these alternative control strategies, the steady state gains from the manipulated inputs to outputs x and S_Y are almost same to each other, the steady state gains from the manipulated inputs to output S_L in control strategy 2 are little bit higher than in control strategy 1. The steady-state gains from F_{in1} to S_Y, from F_{in2} to S_Y and from F_{filter} to S_Y are zeros which means that S_Y only depends on F_{out}. The cell concentration x is sensitive to both the feed limiting substrate flow rate F_{in1} and the cell production flow rate F_{out}, but rather insensitive to F_{filter} and F_{in2}. Flow rates F_{in1}, F_{in2} and F_{filter} have a large effect on S_L.

The frequency-dependent plots of G1 and G2 shown in Fig. (7-8) are also very similar to each other.

Now we look at the steady-state RGA values and CLDG values,

$$\Lambda_1(0) = \begin{bmatrix} 1.02 & -0.02 & 0.00 \\ -0.02 & 1.02 & 0.00 \\ 0.00 & 0.00 & 1.00 \end{bmatrix}; \quad \Lambda_2(0) = \begin{bmatrix} 1.02 & -0.02 & 0.00 \\ -0.02 & 1.02 & 0.00 \\ 0.00 & 0.00 & 1.00 \end{bmatrix}$$

$$\Delta_1(0) = \begin{bmatrix} 0.61 & 0.00 & 0.00 & 1.00 & 0.21 & -1.02 \\ 0.00 & 11.18 & 0.00 & 0.01 & 3.81 & -18.63 \\ 0.00 & 0.00 & 1.47 & 0.00 & 0.50 & -2.44 \end{bmatrix}; \quad \Delta_2(0) = \begin{bmatrix} 0.61 & 0.00 & 0.00 & 1.00 & 0.21 & -1.02 \\ 0.00 & 11.41 & 0.00 & 0.70 & 3.88 & -18.95 \\ 0.00 & 0.00 & 1.47 & 0.00 & 0.50 & -2.44 \end{bmatrix}$$

The frequency-dependent plots of RGA and CLDG (only the elements with magnitudes larger than one) are shown in Fig.(9-12). We see that both the steady state RGA values and the frequency-dependent plots of RGA are same in two alternative control strategies. The steady state CLDG and the frequency-dependent plots of CLDG are almost same in the two alternative control strategies. The CLDG show that for all three outputs, the most difficult disturbance to reject is changes in the parameter μ_m and the required bandwidths for controlling x, S_L and S_Y respectively are also same in the two alternative control strategies, the required bandwidth for controlling x is about 0.06 rad/hr (time constant of 17 hours), the required bandwidth for controlling S_L is about 200 rad/hr (very fast time constant of 0.3 minute) and the required bandwidth for controlling S_Y is about 0.2 rad/hr (time constant of 5 hours)

Therefore **we concluded** that, based on the controllability analysis, the nonlimiting substrate feed flow rate F_{in2} and the filtrate bleeding rate F_{filter} have same effect on outputs x, S_L and S_Y from control point of view. On the other hand, although increasing F_{in2} and increasing F_{filter} have same effect on the reactor volume control, from biotechnology point of view increasing F_{in2} means that more *fresh* media are put into the loop reactor and increasing F_{filter} means that more *used* media are taken out of the loop reactor and thus obviously the later is more economical way to adjust the reactor volume. Consequently we chose F_{filter} to control the reactor volume and the rest three flow rates F_{in1}, F_{in2} and F_{out} to control outputs x, S_L and S_Y.

We now proceed with control structure selection by following the paring rules as described in Section 3.1. From the steady state RGA values, we first see that no significant interaction problems exist between these control loops of x, S_L and S_Y. Furthermore, this plant (corresponding to the given parings $u_1 - y_1$, $u_2 - y_2$ and $u_3 - y_3$) is Decentralized Integral Controllable (DIC) since $\sqrt{\lambda_{11}(0)} + \sqrt{\lambda_{22}(0)} + \sqrt{\lambda_{33}(0)} > 1$ (Yu and Fan, 1990). The RGA values of this plant are small, thus the Rule 1 is satisfied. Based on the Rule 2, we should avoid *paring ij* with negative values

of the steady-state RGA, and thus using F_{in1} to control S_L should be avoided even it has a large steady-state gain. From the Rule 3, we should avoid the paring $u_1 - y_3$ (or $u_2 - y_3$) since g_{31} (or g_{32}) has a zero at the origin.

In summary, we choose $u_1(F_{in1})$ to control $y_1(x)$, $u_2(F_{in2})$ to control $y_2(S_L)$ and $u_3(F_{out})$ to control $y_3(S_Y)$, in order to have positive steady-state RGA values. We also see, from the CLDG, that in this control structure no problems with input constraints exist as all $|g_{ii}| > |\delta_{ik}|$ for $i = 1, 2, 3$ and $k = 1, ..., 5$. This control structure selection is in agreement with industrial practice.

One may argue that it seems having an alternative control structure with parings $u1-y3$, $u2-y2$ and $u3 - y1$ since these parings corresponding to relative gains close to 1 in the higher frequency region (see Fig. (9)). However the obvious reason for not choosing the paring $u1(F_{in1}) - y3(S_Y)$ is that at steady state S_Y is independent of F_{in1} as above discussed. About the paring $u3(F_{out})-y1(x)$, from the maximization of productivity point of view, using F_{out} to control x is unfavorable for maximization of the cell productivity ($P = F_{out}x$) as x varies in the opposite direction to F_{out}, i.e., to increase x we have to decrease F_{out}. We have already discussed this issue in detail in the section 4.2 about maximizing cell productivity.

4.3.2 Operating Point II

This operating point corresponds to the maximum cell productivity. Since the reactor is operating closer to washout, tighter control is needed to maintain stability. We have

$$G(0) = \begin{bmatrix} 3.30 & -0.30 & -9.86 \\ -60.18 & 60.17 & 125.16 \\ 0.00 & 0.00 & 33.29 \end{bmatrix}$$

We note immediately that the outputs are much more sensitive to the manipulated input F_{out} than in operating point No. I.

The steady-state RGA values and CLDG values are given as following,

$$\Lambda(0) = \begin{bmatrix} 1.10 & -0.10 & 0.00 \\ -0.10 & 1.10 & 0.00 \\ 0.00 & 0.00 & 1.00 \end{bmatrix}$$

$$\Delta(0) = \begin{bmatrix} 0.66 & 0.00 & 0.00 & 1.00 & 0.05 & -1.1 \\ 0.00 & 12.03 & 0.00 & 0.01 & 0.90 & -20.05 \\ 0.00 & 0.00 & 6.66 & 0.00 & 0.50 & -11.10 \end{bmatrix}$$

The frequency-dependent plots of RGA and CLDG (only the elements with magnitudes larger than one) are shown in Fig. (13-15).

The steady state RGA values show again that there still not exist significant interaction problems between these control loops of x, S_L and S_Y. The CLDG show that for all three outputs, the most difficult disturbance to reject is still changes in the parameter μ_m. The required bandwidth for controlling x is about 0.03 rad/hr (time constant of 33 hours), the required bandwidth for controlling S_L is about 200 rad/hr (very fast time constant of 0.3 minute) and the required bandwidth for controlling S_Y is about 0.5 rad/hr (time constant of 2 hours). In this case, the output S_Y is much sensitive to disturbances in flow rate F_{out} and parameter μ_m than in operating point I.

We still prefer the parings u_1-y_1, u_2-y_2 and u_3-y_3 because of positive steady-state RGA values and without input constraint problems with this control structure (all $|g_{ii}| > |\delta_{ik}|$ for $i = 1, 2, 3$ and $k = 1, ..., 5$).

In summary, the *choice of parings* appears to be unaffected by changes in the operating point, as all RGA values are smaller in wide frequency range and the RGA values corresponding to the chosen parings are positive at steady state.

4.4 Practical issue

4.4.1 Partial control of the loop reactor

Practically to implement a 3×3 control system of bioreactors is expensive and very difficult because of the lack of accurate mathematical models which describe the cell growth and the lack of reliable on-line sensors which can detect the state variables. Next main consideration is on whether one may achieve acceptable control performances of all three outputs by controlling only one of them. A useful tool when considering issue 2 is the partial disturbance gain (PDG) (Skogestad and Wolff, 1992) which is the effect of a disturbance on the uncontrolled output when the controlled outputs are kept constant,

$$PDG_{ijk} = \left(\frac{\partial y_i}{\partial d_k}\right)_{u_j, y_{l \neq i}} = [G^{-1}G_d]_{jk}/[G^{-1}]_{ji}$$

where y_i— uncontrolled output

u_j— left in manual

$y_{l \neq i}$— other outputs under perfect control

For a particular disturbance d_k one should check if there exists a particular paring of y_i and u_j with the PDG_{ijk} less than 1 in magnitude such that the effect of disturbance d_k on the uncontrolled output y_i is acceptable. For simultaneous disturbances the worst overall effect may be evaluated by taking the sum of element magnitudes for each "pairing". This gives rise to a combined PDG-matrix, denoted C_{PDG}, with elements

$$[C_{PDG}]_{ij} = \sum_k |[PDG]_{ijk}|$$

It is desirable to find an "uncontrolled paring" u_j - y_i for which the C_{PDG} - element is less than 1.

At steady state the matrix C_{PDG} of combined partial disturbance gains is

$$C_{PDG}(0) = \begin{bmatrix} 2.82 & 1.81 & \infty \\ 2868.8 & 33.03 & \infty \\ 6.29 & 4.41 & 4.41 \end{bmatrix}$$

Then we can not find any pairings that may be left uncontrolled and still get acceptable control performance under the worst overall effects of all disturbances, because each element in C_{PDG} matrix is larger than 1. The C_{PDG} also indicates that we can not use F_{in1} to control S_Y, otherwise the system may go unstable when other loops open ($C_{PDG_13} = C_{PDG_23} = \infty$).

4.4.2 Filter-switch problem

Practically, there are two filters equipped in this loop reactor but normally only one is used. When the working filter is clotted, it is switched to another filter which is filled with pure water and this results in the 20 % decrease in cell concentration. Originally, it was suggested to keep F_{out} unchanged during filter-switch, but this yields long period of oscillations in x, and the time needed for x back to the desired value is about 30 hours as shown in Fig. 16. Instead, we propose to stop production ($F_{out} = 0$) for about 2 hours and then x returns to the desired value very quickly as shown in Fig. 17.

5 Simulation results

In this section we present nonlinear simulation results to compare with the controllability analysis results presented in the previous section. All simulations are for operating point No. I and simple

PI controllers are used for the controlled outputs. In all simulations we consider the step responses to the combined disturbances in parameters of 10% decrease in the yield $Y_{x/Y}$ from 0.08 to 0.072 [g/g], 10% increase in K_s from 0.0343 to 0.0377 [g/l] and 10% decrease in specific growth rate (μ_m) from 0.141 to 0.127 [1/h].

In Fig. (18-19), $x(y_1)$ is controlled by $F_{in1}(u_1)$, $S_L(y_2)$ is controlled by $F_{in2}(u_2)$ and $S_Y(y_3)$ is controlled by $F_{out}(u_3)$. This control scheme works well against the combined disturbances in parameters as all controlled outputs remain at their desired steady states without violating the input constraints. In Fig. (20-21), $x(y_1)$ is controlled by $F_{out}(u_3)$, $S_L(y_2)$ is controlled by $F_{in2}(u_2)$ and $S_Y(y_3)$ is controlled by $F_{in1}(u_1)$. This control scheme also works well against the combined disturbances. Using F_{in1} to perfectly control S_Y is feasible because other outputs x and S_L are also perfectly controlled by other manipulated inputs and no input left in manual.

The next Figs. show the step responses to the combined disturbances under partial control. In Fig. (22-23), only x is controlled by F_{in1}, S_L and S_Y are uncontrolled with F_{in2} and F_{out} left in manual. x is perfectly controlled without violating the input constraint of F_{in1}, the uncontrolled S_L is almost back to its desired steady state after several hours. However the uncontrolled S_Y exceeds its allowed bound. In Fig. (24-25), only x is controlled by F_{out}, S_L and S_Y are uncontrolled with F_{in1} and F_{in2} left in manual. The uncontrolled S_Y remains within its allowed bound, but S_L goes to much higher concentration and then result in losing more substrate LA. In Fig. (26-27), x and S_L are uncontrolled with F_{in1} and F_{in2} left in manual, and S_Y is controlled by F_{out}. After long period of oscillation, S_Y may be controlled at the desired value and the deviation of the uncontrolled x from its desired value may also be acceptable, but similar to the case shown in Fig s4, S_L goes to much higher concentration. In Fig. (28-29), S_Y is controlled by F_{in1} and x and S_L are uncontrolled with F_{in2} and F_{out} left in manual. The uncontrolled x decreases quickly and eventually down to zero and then the reaction will stop: F_{in1} has to be continuously lowered in order to try to keep S_Y constant, however, it is not possible to keep S_Y constant in the long run while F_{out} is unchanged because S_Y is independent of F_{in1} at steady state, and finally F_{in1} will reach 0 and results in a failure of the reactor. This simulation result also confirm the validity of the conclusion from the controllability analysis, i.e., the pairing $F_{in1}(u_1) - S_Y(y_3)$ should be avoided. Comparing these four partial control schemes, if the required control performences for S_L and S_Y are lower, for example, the allowed maximum changes for them are 40 % of their desired value, then we can only control x and the uncontrolled S_L and S_Y can remain within their allowed bounds.

6 On-line estimation of cell concentration

The knowledge of fermentation process state variables is crucial in any type of control scheme. Unfortunately, on-line measurement of the important state variables in fermentations, particularly cell concentration, remains a difficult problem. However a number of secondary or environmental variables can be on-line measured conventionally, such as pH, and CO_2 and O_2 in the exhaust gas. In propionic acid bacteria fermentation, CO_2 is the only gas produced. Further the CO_2 concentration is related to the cell growth rate. We have another available on-line measurement of secondary variable, that is base addition rate which is found to be possibly also related to the cell growth rate from experiment data analysis. Based on two assumptions:

- pH change in fermenter is caused only by the organic acids produced from yeast extract.
- No accumulation of base in fermenter as the dynamics of compensating pH change by adding base solution is very fast compared to the cell growth dynamics.

We have the dynamic equation for base consumption,

$$\frac{db}{dt} = -\frac{1}{Y_{x/base}}\mu x + \frac{F_{in3}}{V} b_f = 0 \tag{13}$$

Then it is now possible to on-line estimate the cell growth rate as a function of the directly on-line measurable variable F_{in2}:

$$\mu x = Y_{x/base}\frac{F_{in3}}{V}b_f \tag{14}$$

Where

$Y_{x/base}$— the cell yield coefficient on the carbon dioxide.

b_f— the feed base concentration.

Further the cell mass concentration can be on-line estimated in this way.

As discussed by Stephanopoulos and San (1984), the Extended Kalman filter (EKF) can be applied to fermentation state estimation. Thus we use EKF for on-line state estimation in propionic acid bacterium fermentation process.

The dynamic equations given in Section 2 are written in vector form:

$$\frac{dX}{dt} = f(X,t),\ X = [x \quad S_L \quad S_Y \quad c]^T \tag{15}$$

Measurement equation:

$$Y = H^T X = \begin{bmatrix} \mu & 0 & 0 & 0 \\ 0 & 0 & 0 & 1 \end{bmatrix} X = \begin{bmatrix} \mu x \\ c \end{bmatrix} \tag{16}$$

After discretization (let $X(t) = X_K$, $X(t+T) = X_{K+1}$):

$$X_{K+1} = X_K + Tf(X_K) = F(X_K) \tag{17}$$

$$Y_K = H^T X_K \tag{18}$$

After linearization and incorporation of process noise W_K and measurement noise V_K into equations:

$$X_{K+1} = A_K X_K + B(\hat{X_K}) + W_K \tag{19}$$

$$Y_K = H^T X_K + V_K \tag{20}$$

Where $\hat{X_K}$ stands for known or estimated state values at time K,

$$A_K = \frac{\partial F}{\partial X}_{X=\hat{X_K}} \tag{21}$$

$$B(\hat{X_K}) = F(\hat{X_K}) - A_K \hat{X_K} \tag{22}$$

Based above model, the corresponding EKF equations are given in following:

$$\hat{X_K} = \hat{X_{k|k-1}} + L_K(Y_K - H^T \hat{X_{k|k-1}}) \tag{23}$$

$$\hat{X_{k+1|k}} = A_K \hat{X_K} + B(\hat{X_K}) \tag{24}$$

$$L_K = P_{K|K-1}H(H^T P_{K|K-1}H + R_K)^{-1} \tag{25}$$

$$P_K = (I - L_K H^T)P_{K|K-1} \tag{26}$$

$$P_{K+1|K} = A_K P_K (A_K)^T + Q_K \tag{27}$$

Initial condition: $P_{0|-1} = 0$, $\hat{X_{0|-1}} = [x_0 \quad S_{L_0} \quad S_{Y_0} \quad c_0]^T$.

Here we assume that the process noise W_K and the measurement noise V_K are two white-noise processes of intensity Q and R separately as shown in the upper part of Fig. 30, the simulation results are shown in the lower part of Fig. 30. A good agreement is observed between the true state values and the estimated state values. Therefore the cell concentration, and other state variables can be on-line estimated by applying the EKF from these two available on-line measurement variable CO_2 concentration and base addition rate.

7 Conclusions and further study

By using simple frequency-dependent tools such as the relative gain array (RGA) and the closed loop disturbance gain (CLDG), we choose the growth-limiting substrate feed flow rate F_{in1} to control the cell concentration x, the nonlimiting substrate feed flow rate F_{in2} to control the nonlimiting substrate concentration S_L and the cell production rate F_{out} to control the growth-limiting substrate concentration S_Y, in order to have positive steady-state RGA values and to avoid input constraints. This selected control structure is in agreement with industrial practice. The control structure selection appears to be unaffected by changes in the operating point.

For maximization of cell productivity, we suggested that in the loop reactor the better way to get as higher as possible cell productivity is to increase F_{out} together with adjusting F_{in1} to keep x at the desired high concentration.

Based on the developed estimation model in this work that describes cell concentration as a function of the CO_2 concentration and the base addition rate , cell concentration can be on-line estimated from these two on-line measurements by applying the extended Kalman filter. From simulation results, a good agreement is observed between the true values and the estimated values. It is clear that a reasonably good model is essential in order to take full advantage of the extended Kalman filtering theory. At present, however, for real fermentation process the accurate mathematical model, which describe the cell growth and the metabolization of microoganism, is not available due to the high complexity of biological systems as they involve living organisms. Therefore the values of the model kinetic parameters should be on-line updated in order to match the model to changes in the behavior of the fermentation process, especially the saturation constant K_s in the Monod kinetics which has the big effect on the steady state behavior and dynamic behavior of this process. Then by incorporating off-line measurements on cell mass and other state variables, an adaptive cell mass estimator can be developed where the model kinetic parameters are updated whenever a new off-line measurement is available and in between off-line samples, these parameters are kept constant and used along with the on-line measurements to estimate the cell mass concentration and other state variables.

References

[1] Grosdidier, P., M. Morari and B.R. Holt, 1985, "Closed-Loop Properties from Steady-State Gain Information", *Ind. Eng. Chem. Fundam.*, 24, p. 221-235.

[2] Hovd, M. and S. Skogestad, 1992, "Simple Frequency-Dependent Tools for Control System Analysis, Structure Selection and Design", *Automatica*, 28, 5, p. 989-996.

[3] Skogestad, S. and M. Morari, 1987b, "Implications of large RGA elements on control performance", *Ind. Eng Chem. Res.*, 26, 11, p. 2323-2330.

[4] Skogestad, S., and E. A. Wolff, 1992, "Controllability measures for disturbance rejection", *Proc. of IFAC Workshop on Interactions Between Process Design and Control*, London, UK.

[5] Stephanopoulos, G. and K. -Y. San, 1984, "Studies on on-line bioreactor identification. I. Theory", *Biotechnol. Bioeng*, 26, p. 1176-1188.

[6] Yu, C.-C. and Fan, M.K.H., 1990, "Decentralized Integral Controllability and D-Stability", *Chem. Eng. Sci.*, 45, 11, p. 3299-3309.

FIGURE LIST
Fig.1: ~/latex/AICHE94/fig/loopreactor.ps

Fig.2: ~/latex/AICHE94/fig/ss_Fout.eps
Fig.3: ~/latex/AICHE94/fig/ss_Fin1.eps
Fig.4: ~/latex/AICHE94/fig/ss_Fin2.eps
Fig.5: ~/latex/AICHE94/fig/ss_Ffilter.eps

Fig.6: ~/latex/AICHE94/fig/optima.eps

Fig.7: ~/latex/AICHE94/fig/opI_G.eps
Fig.8: ~/latex/AICHE94/fig/opI_Gf5a.eps
Fig.9: ~/latex/AICHE94/fig/opI_RGA.eps
Fig.10: ~/latex/AICHE94/fig/opI_RGAf5a.eps
Fig.11: ~/latex/AICHE94/fig/opI_CLDG.eps
Fig.12: ~/latex/AICHE94/fig/opI_CLDGf5a.eps

Fig.13: ~/latex/AICHE94/fig/opII_G.eps
Fig.14: ~/latex/AICHE94/fig/opII_RGA.eps
Fig.15: ~/latex/AICHE94/fig/opII_CLDG.eps

Fig.16: ~/latex/AICHE94/fig/filterswitch_fig2.eps
Fig.17: ~/latex/AICHE94/fig/filterswitch_fig1.eps

Fig.18: ~/latex/AICHE94/fig/pairing1_fig1.eps
Fig.19: ~/latex/AICHE94/fig/pairing1_fig2.eps
Fig.20: ~/latex/AICHE94/fig/pairing2_fig1.eps
Fig.21: ~/latex/AICHE94/fig/pairing2_fig2.eps

Fig.22: ~/latex/AICHE94/fig/F22_x_fig1.eps
Fig.23: ~/latex/AICHE94/fig/F22_x_fig2.eps
Fig.24: ~/latex/AICHE94/fig/F6_x_fig1.eps
Fig.25: ~/latex/AICHE94/fig/F6_x_fig2.eps
Fig.26: ~/latex/AICHE94/fig/F6_sy_fig1.eps
Fig.27: ~/latex/AICHE94/fig/F6_sy_fig2.eps
Fig.28: ~/latex/AICHE94/fig/F22_sy_fig1.eps
Fig.29: ~/latex/AICHE94/fig/F22_sy_fig2.eps
Fig.30: ~/latex/AICHE94/fig/estimate.eps

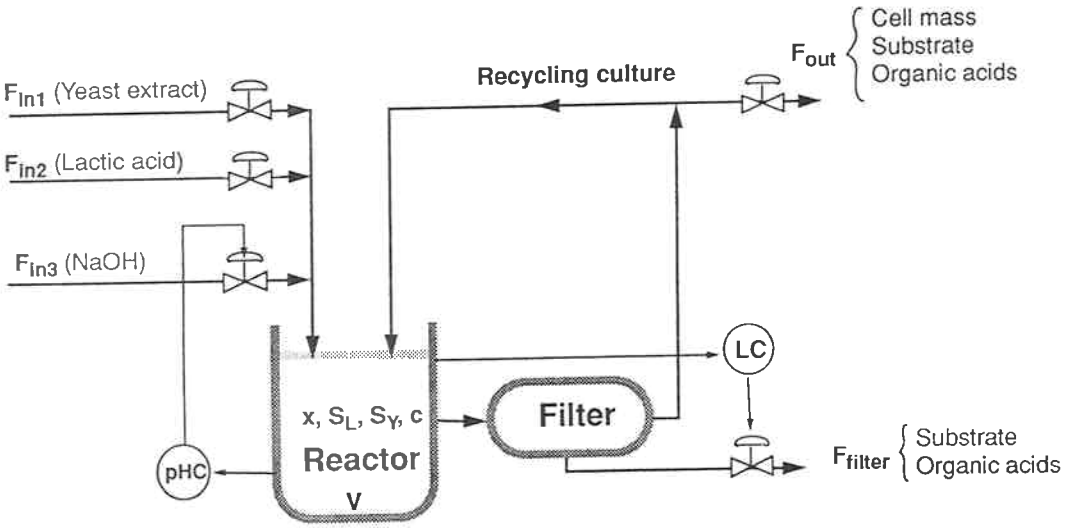

Figure 1: A biochemical loop reactor with cell mass recycle.

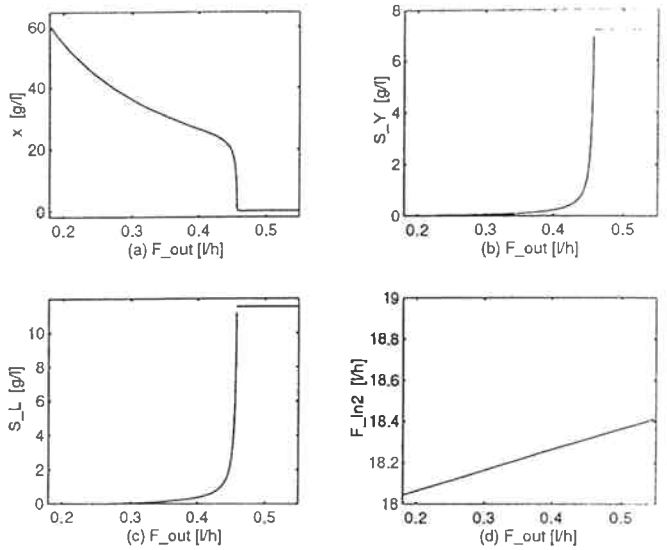

Figure 2: Steady state values of x, S_L and S_Y as functions of F_{out}.

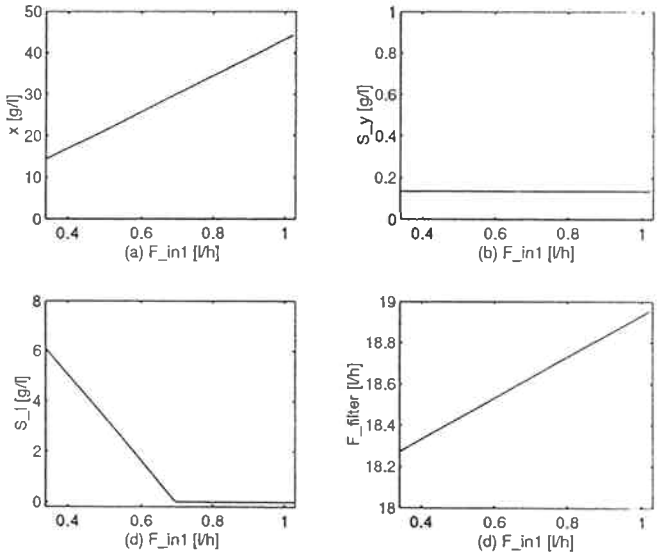

Figure 3: Steady state values of x, S_L and S_Y as functions of F_{in1}.

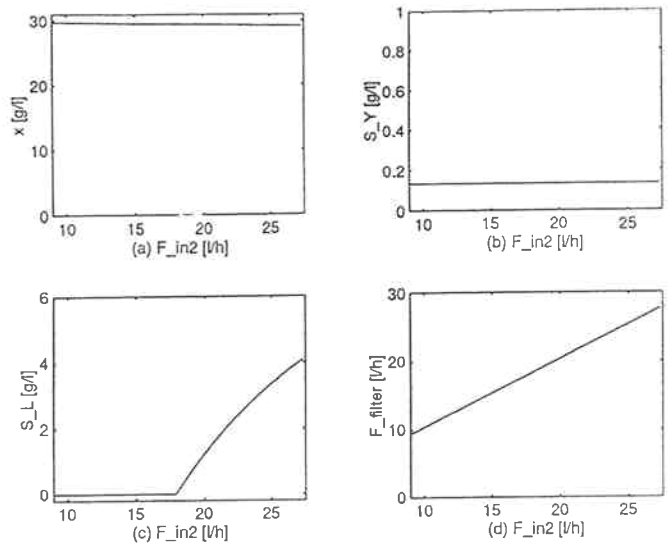

Figure 4: Steady state values of x, S_L and S_Y as functions of F_{in2}.

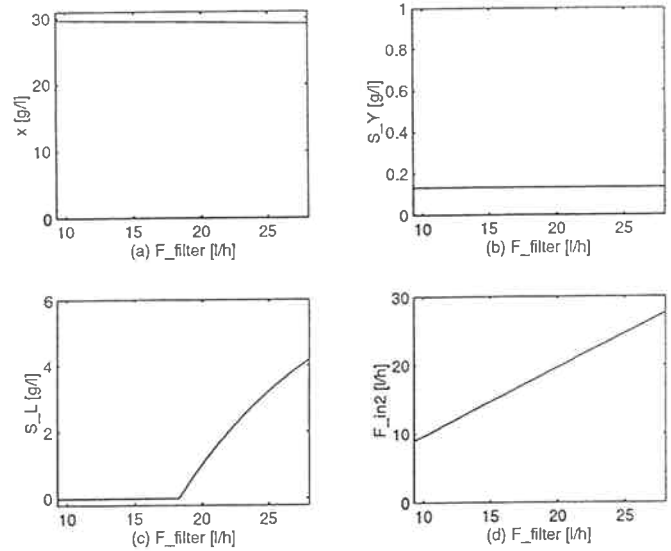

Figure 5: Steady state values of x, S_L and S_Y as functions of F_{filter}.

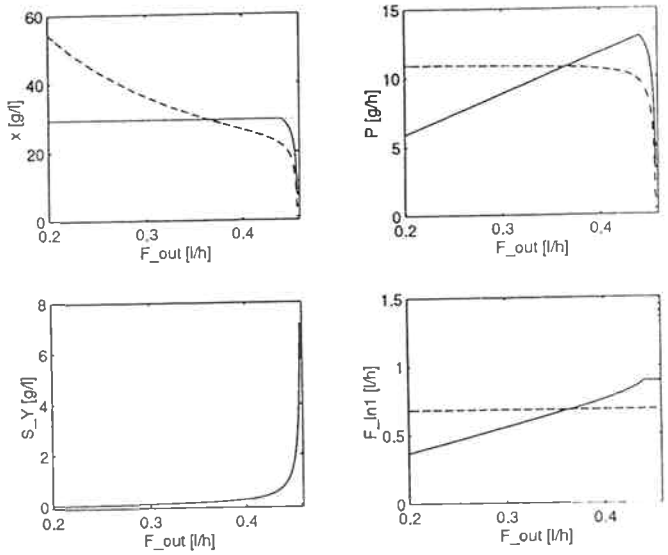

Figure 6: Maximization of cell productivity in case 1 (dashed) and case 2 (solid)

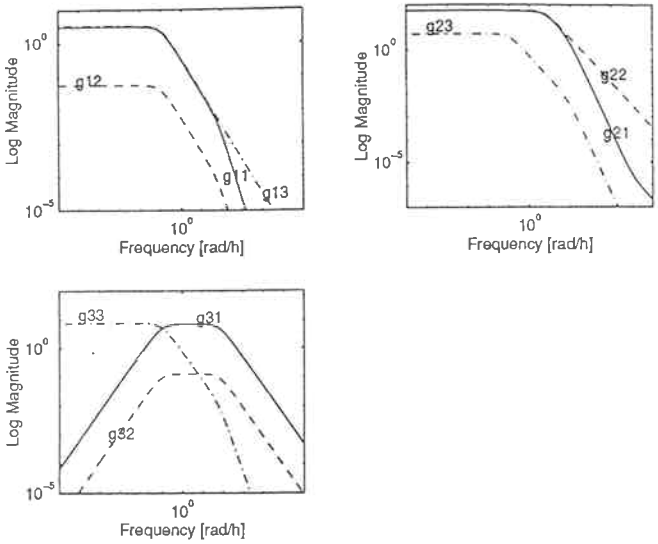

Figure 7: Frequency-dependent plots of G_1 in operating point I

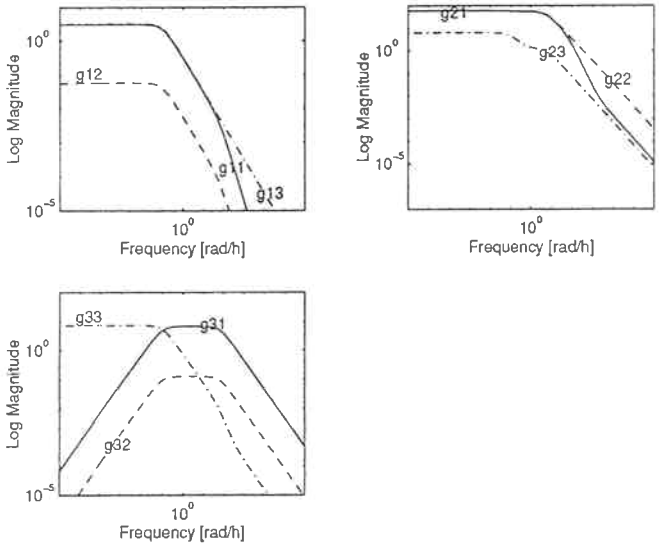

Figure 8: Frequency-dependent plots of G_2 in operating point I

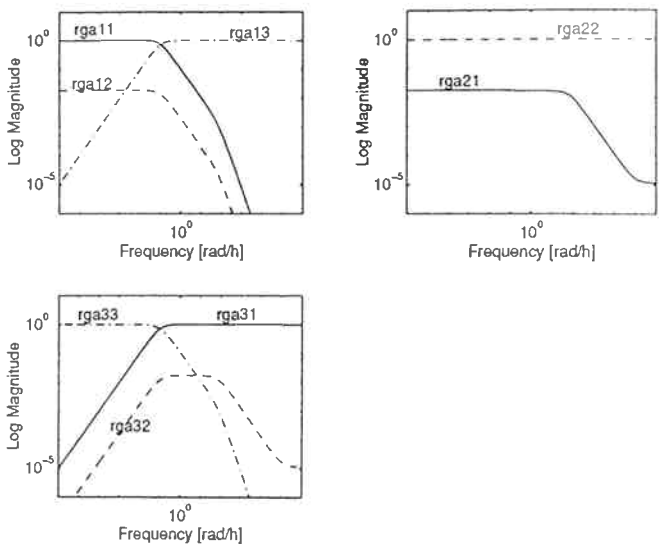

Figure 9: Frequency-dependent plots of RGA_1 in operating point I

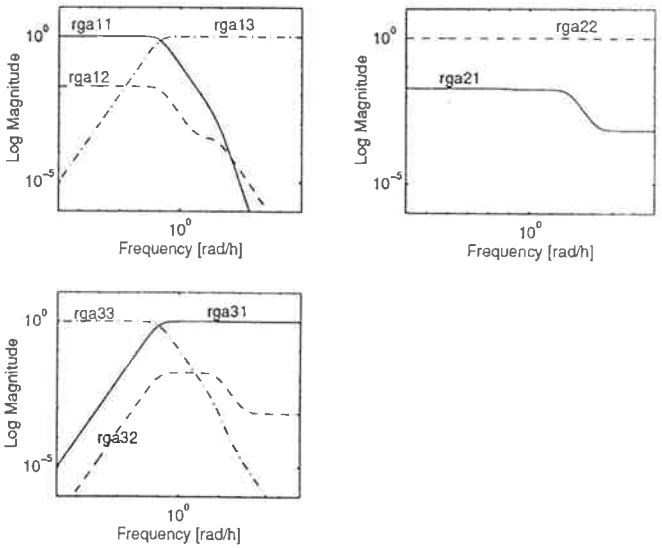

Figure 10: Frequency-dependent plots of RGA_2 in operating point I

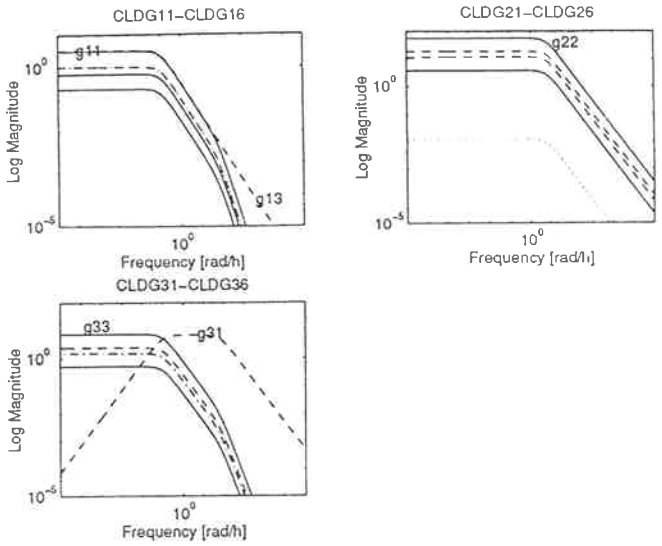

Figure 11: Frequency-dependent plots of $CLDG_1$ in operating point I

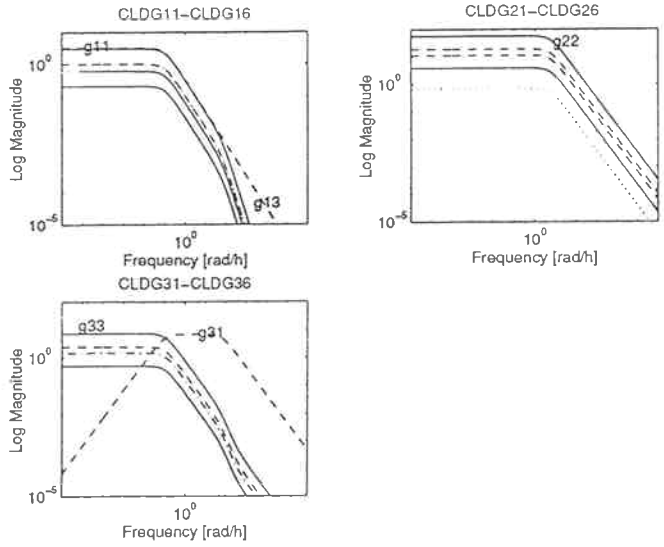

Figure 12: Frequency-dependent plots of $CLDG_2$ in operating point I

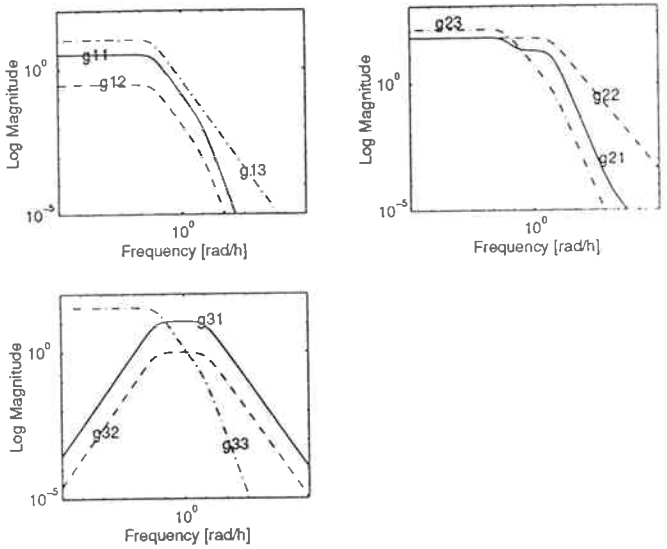

Figure 13: Frequency-dependent plots of G in operating point II

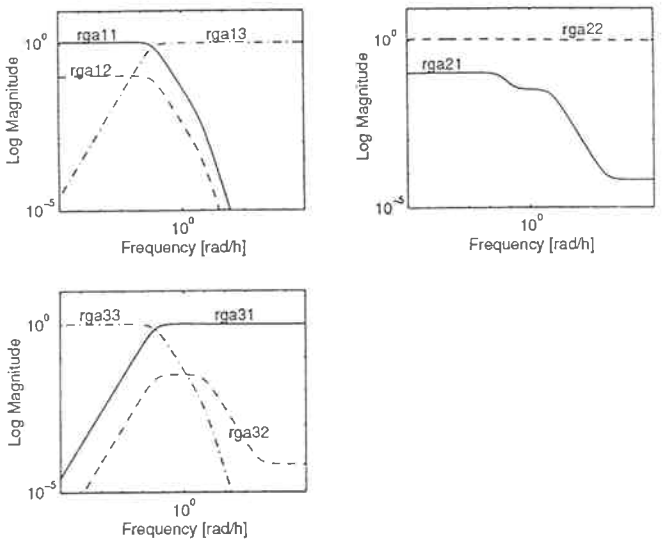

Figure 14: Frequency-dependent plots of RGA in operating point II

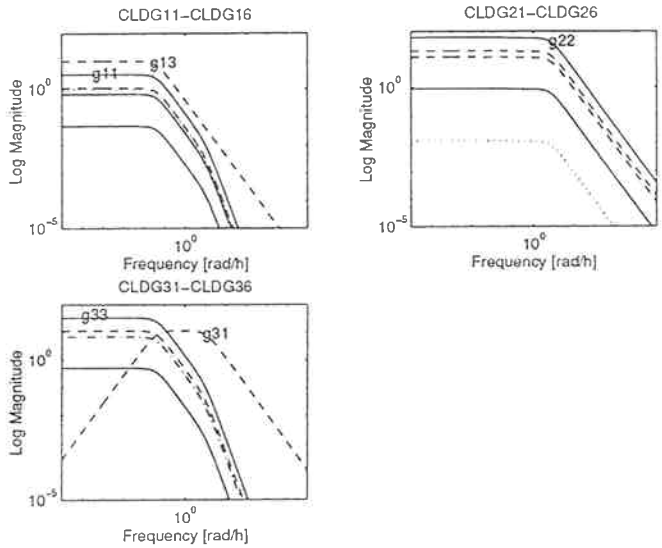

Figure 15: Frequency-dependent plots of $CLDG$ in operating point II

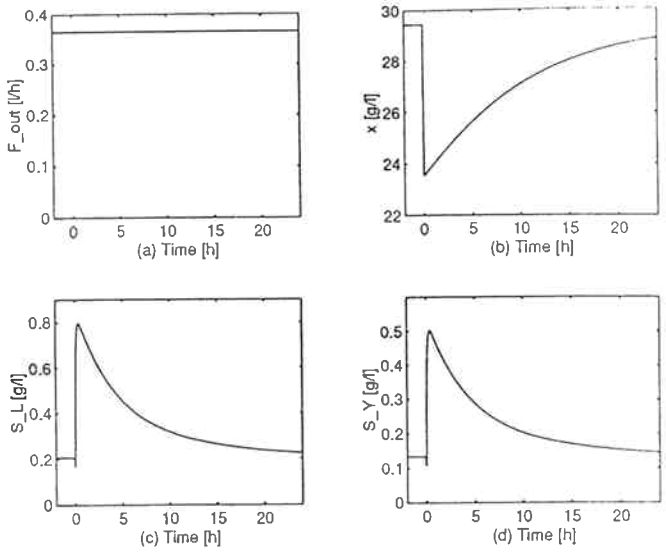

Figure 16: F_{out} unchanged when filter-switch occurs

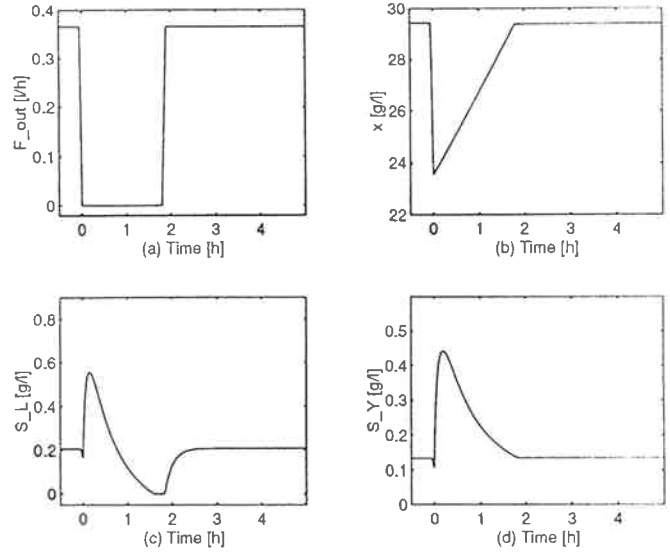

Figure 17: $F_{out} = 0$ for about 2 hours when filter-switch occurs

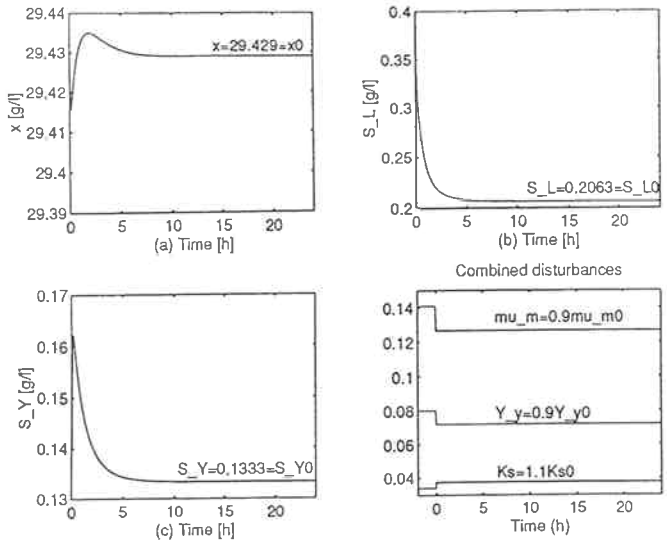

Figure 18: Time responses (outputs) for the combined step disturbances in Y_y, μ_m and K_s, by pairing 1

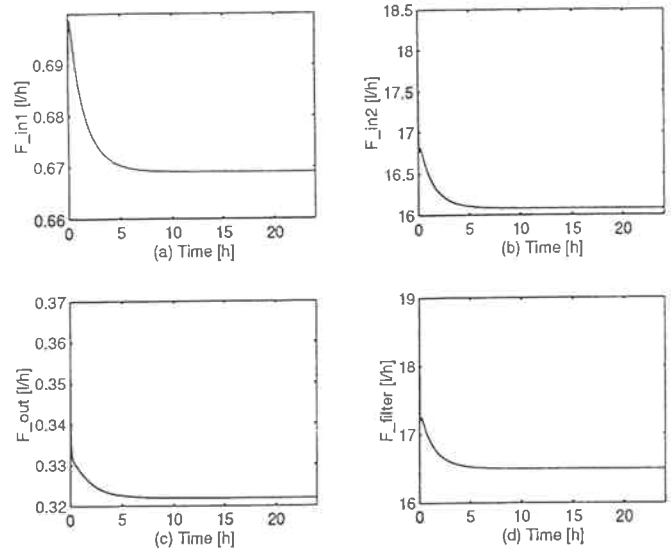

Figure 19: Time responses (control action) for the combined step disturbances in Y_y, μ_m and K_s, by pairing 1

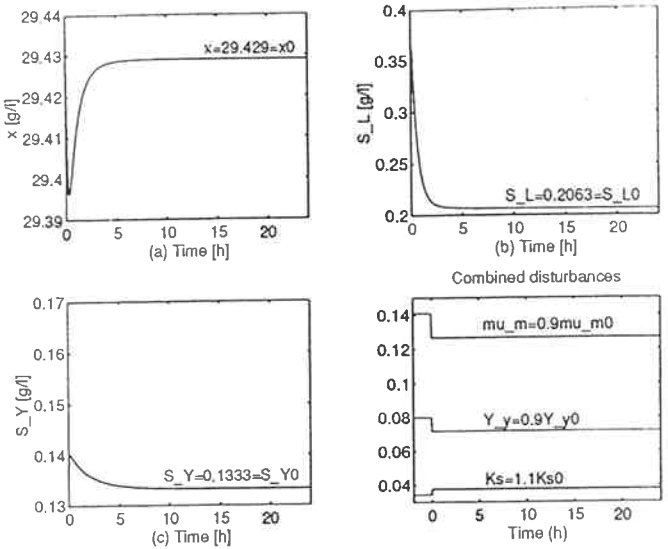

Figure 20: Time responses (outputs) forthe combined step disturbances in Y_y, μ_m and K_s, pairing 2

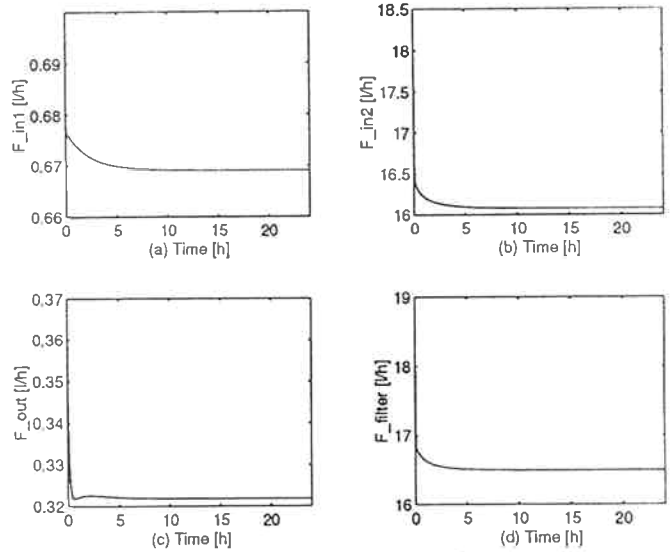

Figure 21: Time responses (control action) for the combined step disturbances in Y_y, μ_m and by pairing 2

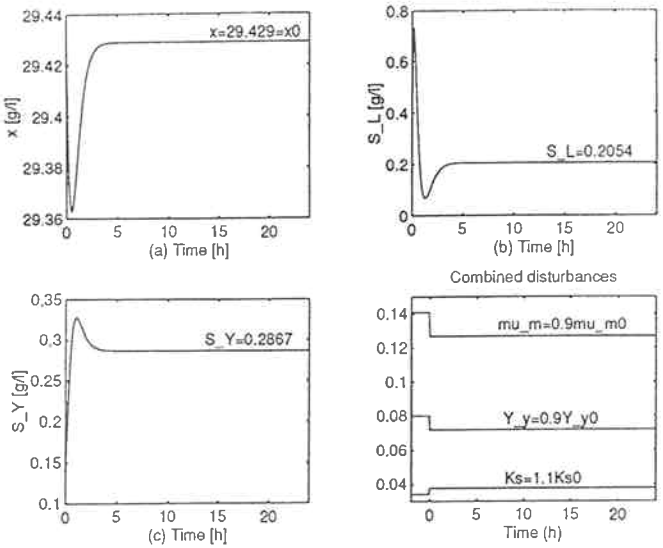

Figure 22: Time responses (outputs) for the combined step disturbances in Y_y, μ_m and K_s, by partial control $F_{in1} \rightarrow x$)

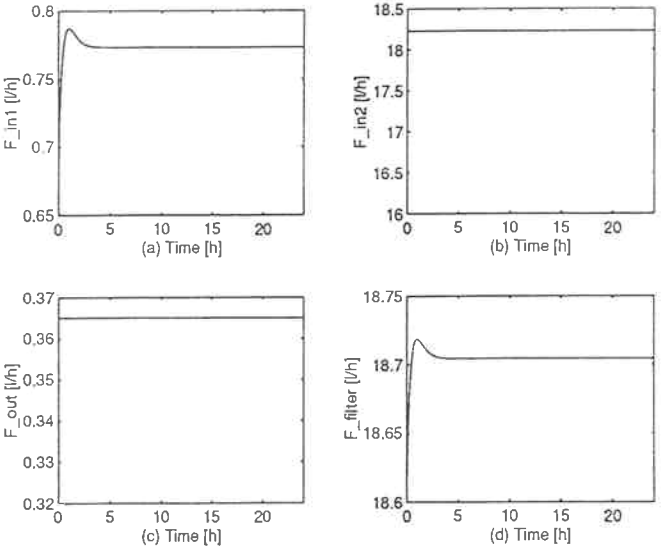

Figure 23: Time responses (control action) for the combined step disturbances in Y_y, μ_m and K_s, by partial control $F_{in1} \rightarrow x$)

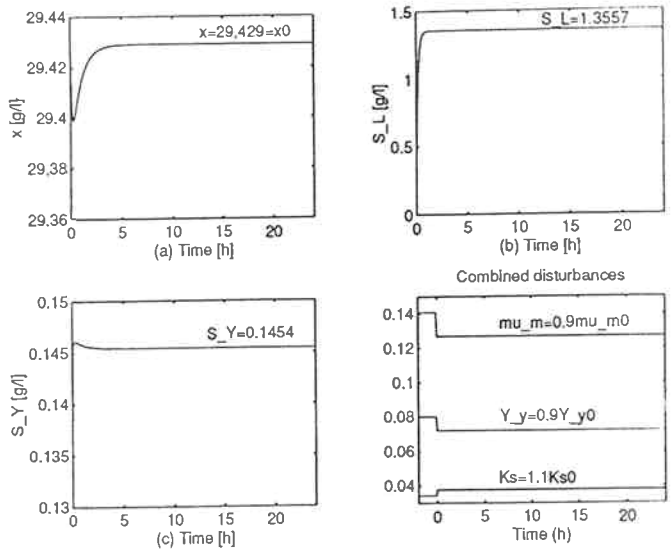

Figure 24: Time responses (outputs) for the combined step disturbances in Y_y, μ_m and K_s, by partial control $F_{out} \rightarrow x$)

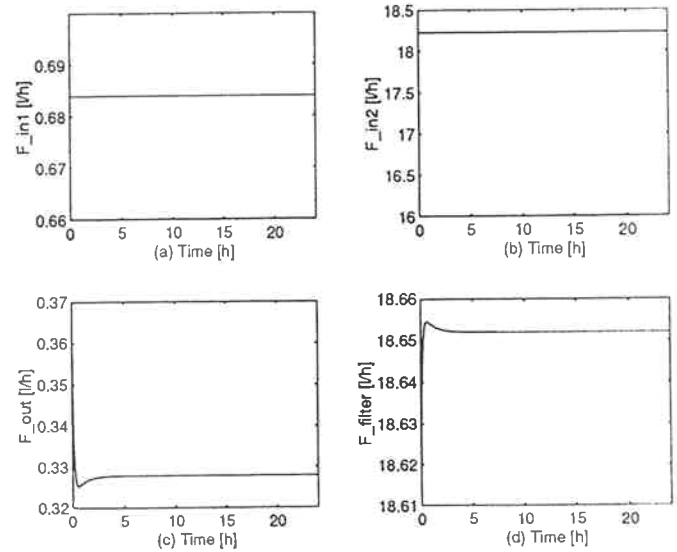

Figure 25: Time responses (control action) for the combined step disturbances in Y_y, μ_m and K_s, by partial control $F_{out} \rightarrow x$)

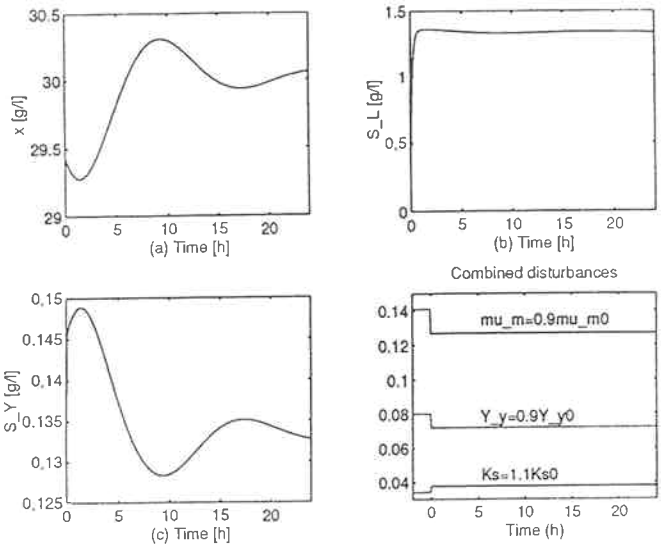

Figure 26: Time responses (outputs) for the combined step disturbances in Y_y, μ_m and K_s, by partial control $F_{out} \rightarrow S_Y$)

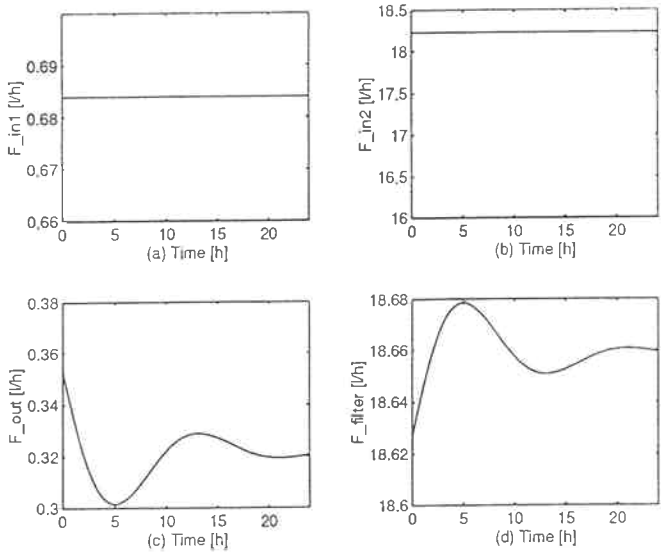

Figure 27: Time responses (control action) for the combined step disturbances in Y_y, μ_m and K_s, by partial control $F_{out} \rightarrow S_Y$)

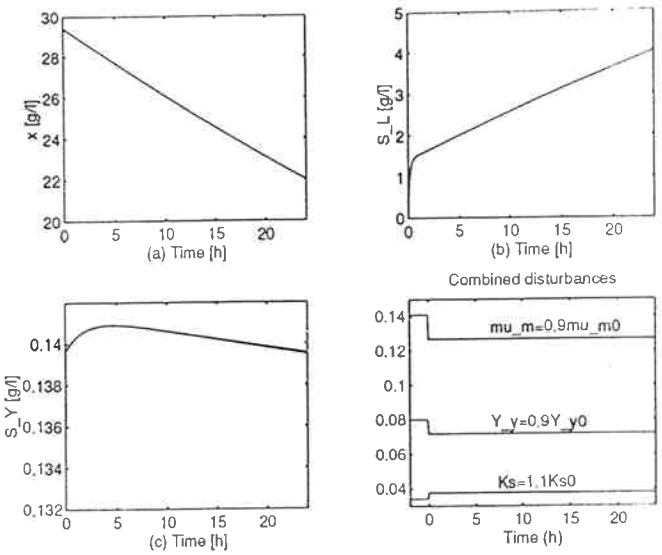

Figure 28: Time responses (outputs) for the combined step disturbances in Y_y, μ_m and K_s, by partial control $F_{in1} \rightarrow S_Y$)

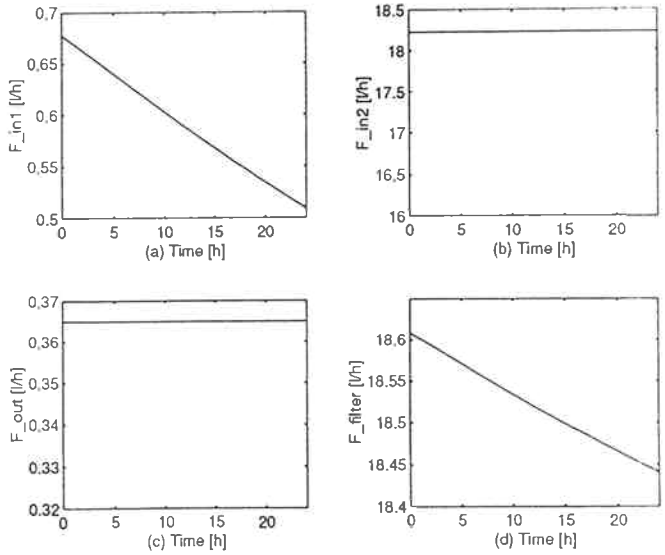

Figure 29: Time responses (control action) for the combined step disturbances in Y_y, μ_m and K_s by partial control $F_{in1} \rightarrow S_Y$)